Lateral Loading Tests on Piled Rafts and Simplified Method to Evaluate Sectional Forces of Piles

J. Hamada[1], T. Tsuchiya[2], T. Tanikawa[3] and K. Yamashita[4]
[1,3,4]*Research and Development Institute, Takenaka Corporation, Chiba, Japan*
[2]*Tokyo Main Office. Takenaka Corporation, Tokyo, Japan*
E-mail: hamada.junji@takenaka.co.jp

ABSTRACT: Both analytical and experimental studies are necessary when developing a seismic design concept for piled raft foundations, especially in highly active seismic areas such as Japan. This paper presents static cyclic lateral loading tests on large-scale piled raft foundations carried out to investigate the influence of vertical load and pile spacing ratios during earthquakes. The test models were pile groups and piled rafts with a concrete footing supported by 16 piles in a 1g field. The results showed that most of the lateral force was carried by raft friction when there was large contact earth pressure beneath the raft, and that piles experienced pulling forces from the raft, behaving like anchors at large deformations. The tested foundations were simulated using a simplified method based on Mindlin's solution, with theoretical equations derived making some approximations and assumptions. The simulated results agreed well with the test results.

Keywords: Piled raft, Lateral loading test, Simplified modeling, Simplified theoretical method

1. INTRODUCTION

In recent years, there has been increasing recognition that the use of piles to reduce raft settlement can lead to considerable economy without compromising foundation safety and performance (Poulos, 2001; Mandolini et al., 2005). A lot of experimental and analytical studies and field measurements on piled raft foundations have been conducted to investigate their settlement behavior and the load-sharing between raft and piles for vertical loading (Katzenbach et al., 2000; Yamashita et al., 2008; Yamashita et al., 2011a; Yamashita et al., 2011b). Much less research has been done on the lateral resistance of piled rafts to seismic loads. A seismic design concept needs to be developed for piled rafts, especially in highly active seismic areas such as Japan. In the conventional design concept for pile groups, all lateral loads are assumed to be carried by the piles only, despite the fact that some of the load is transferred to the soil through the raft by friction. Hence, the required pile diameter is generally large. In the rational design concept for piled rafts, the lateral load is carried by both the piles and by raft friction. In this case, the bending moment in the piles is caused not only by shear force at pile heads but also by ground displacement induced by raft friction as shown in Figure 1.

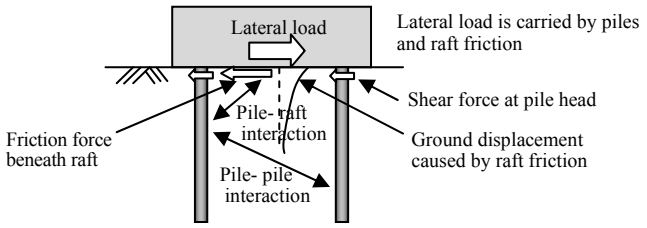

Figure 1 Lateral load distribution within piled raft foundations under lateral load for rational design concept

In the last decade, shaking Table tests (Horikoshi et al., 2003a), static lateral loading tests using centrifuge models (Horikoshi et al., 2003b; Katzenbach & Turek, 2005) and shaking Table tests in 1 g fields (Watanabe et al., 2001; Matsumono et al., 2004a, b; Matsumono et al., 2010) have been carried out. However, the number of model piles was limited in most of these tests, where model superstructures were generally supported by four piles. Recently, a seismic response of a piled raft foundation was successfully recorded during the 2011 off the Pacific Coast of Tohoku Earthquake (Yamashita et al., 2012) and the simulation analysis was conducted using a detailed three-dimensional finite-element model (Hamada et al., 2014).

This paper examines the lateral resistance of piled rafts during seismic events. Static cyclic lateral loading tests of large scale piled rafts were carried out in order to investigate the influence of vertical loading (the contact earth pressure beneath the raft) and the pile spacing ratio s/d (pile spacing/pile diameter) on the sectional forces on the piles and the lateral loading ratio between the piles and the raft. The most important issues in developing a seismic design concept for piled rafts are evaluating the sectional force on the piles and the load sharing ratio between the piles and the raft. The responses of the tested models were simulated using a simplified analytical method based on Mindlin's solution. Theoretical equations were derived for making rough evaluations of the lateral resistance of piled rafts applied several approximations and assumptions.

2. LATERAL LOADING TESTS

2.1 Test Description

Static cyclic lateral loading tests of raft foundations, pile groups and piled raft foundations were conducted in a 1 g field.

2.1.1 Testing devices and measuring devices

The tests were conducted using a large scale container at Takenaka R&D Institute in Japan (Tsuchiya et al., 2001). The container was 2.5 m long, 2.5 m wide and 8 m high. The vertical load was applied using an actuator and the footing was restrained from rotating by means of outer and inner frames.

Axial loads and bending moments on the piles were measured using 184 strain gauges. Earth pressures beneath the raft were also measured using earth pressure gauges.

2.1.2 Model foundation

Figure 2 shows the test set up including the model piled raft, model ground and loading apparatus. Photo 1 shows the model piles set up prior to preparing the model ground and footing. The footing was concrete 1.0 m long, 1.0 m wide and 0.5 m deep, supported by 16 piles for both the pile groups and piled raft foundations. The piles were embedded in the concrete footing. Figuure2(c) shows the embedded depth from 50 to 100 mm and attached strain gauges. Two different pile spacing/pile diameter (s/d) ratios were considered by using model pipes with two different diameters. One model, representing small piles group effect, was made of aluminum pipes having 19 mm outer diameters and walls 1 mm thick, with Young's modulus, E, of 70000 MPa, and second moment of area, I, of 2.30×10^{-9} m^4. Another model, representing large piles group effect, was

made of vinyl chloride pipes having 76 mm outer diameters and walls 2.5 mm thick, with Young's modulus, E, of 3250 MPa, and second moment of area, I, of 3.90×10^{-7} m^4. Neither set of piles' surfaces were improved, but the surface between the raft and the subsoil was rough because the raft was cast in place on model sand. The piles were made not to be rigid. They were not short, having lengths (0.65 m and 1.1 m) that were close to the footing width. Both the lengths and the materials of the piles were selected based on the stiffness of the model soil.

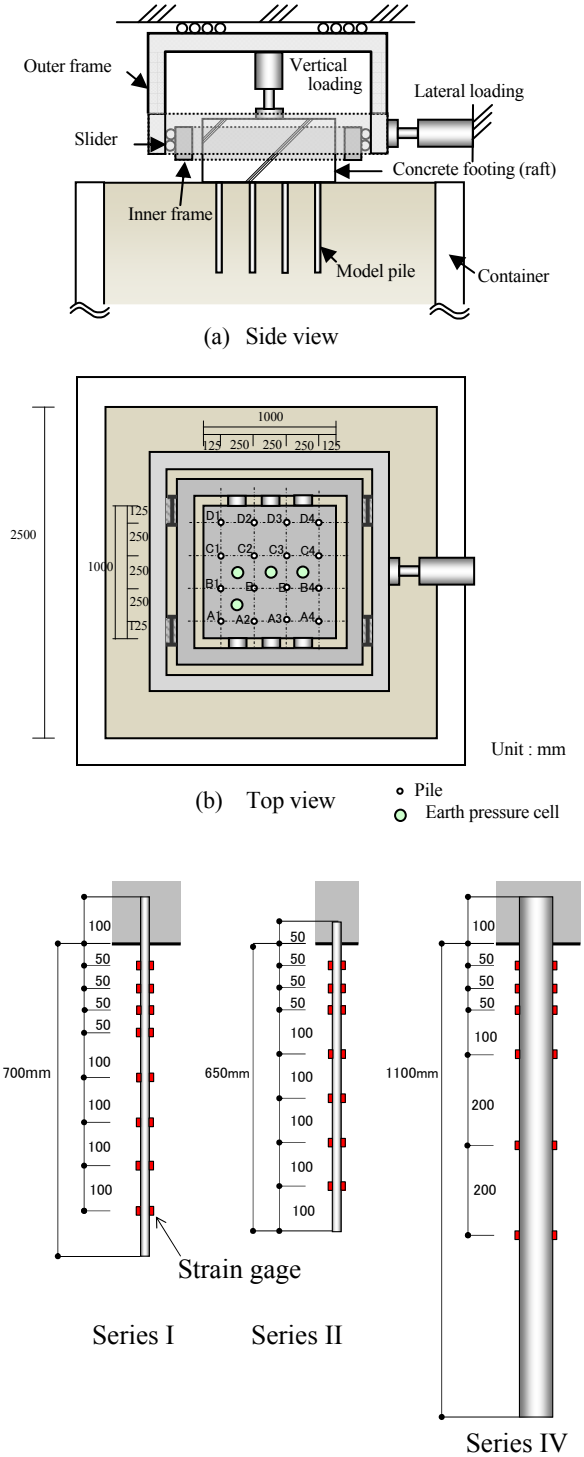

Figure 2 Tests model and loading apparatus

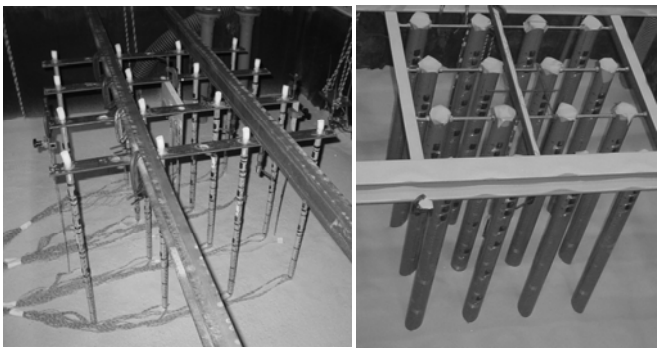

(a) Series II (b) Series IV

Photo 1 Model piles set-up prior to preparing model ground

2.1.3 Model ground

Silica sand No.6 produced in Iide, Yamagata Prefecture, Japan was used as the soil for all test cases. The physical properties of the Iide sand are summarized in Table 1. The internal friction angle estimated from consolidated drained tests was 42 degree at a relative density of 60%. The initial shear modulus at a relative soil density of 80% was proportional to the square root of the confining pressure as given in Figure 3 and Eq. (1), as determined from the initial shear stiffness in a cyclic tri-axial test. Figure 4 shows the relationships between the shear strain γ and normalized shear modulus, G/G_0 of the model sand for different relative densities and confining pressures. The average curves with white squares and white circles (relative densities of 60%, 90% and confining pressure, σ_c of 33kPa) were used as the basic curves for the simulations presented later.

$$G_0=8800\times\sigma_c^{0.53} \quad (kN/m^2) \tag{1}$$

Table 1 Physical properties of model (Iide) sand

50 percent diameter	D_{50}	0.28 mm
Uniformity coefficient	U_c	1.9
Specific gravity of soil particles	G_s	2.64
Minimum density	ρ_{dmin}	1.35 g/cm^3
Maximum density	ρ_{dmax}	1.74 g/cm^3

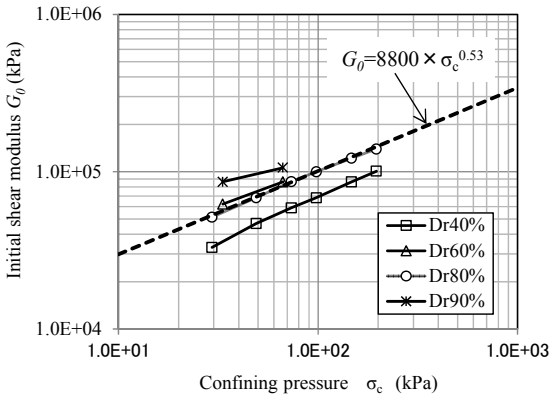

Figure 3 Confining pressure versus initial shear modulus of model sand

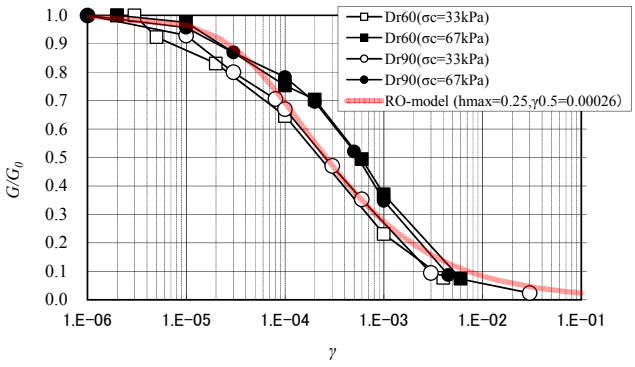

Figure 4 Shear strain versus shear modulus of model sand

2.1.4 Test series

Test cases were conducted in the order listed in Table 2. For series I (pile groups cases), a steel plate was set at each pile toe to restrict the vertical displacement. For series II (piled raft cases with large s/d), the vertical displacement was not restricted. For series III (raft cases), the vertical load was varied. For series IV (piles with small s/d), vinyl chloride pipes of 76mm in diameter were employed. While the pile spacing was set to 0.25 m, s/d ratios for the 19 mm diameter aluminum pipes and 76 mm diameter vinyl chloride pipes were 13 and 3.3, respectively.

The footing was subjected to reversed cycles of lateral loads with increasing amplitudes, controlled by displacement. Two cycles at each displacement amplitude were performed. A maximum lateral displacement of 7 mm was achieved. The shares of the vertical load carried by the piles and the raft before and after the lateral loading are listed in Table 2.

2.1.5 Set up

The procedures for setting up the model ground, model piles and model foundations were as follows. First, a 7.3 m (6.9 m for series IV) thick layer of dry sand was poured into the soil container and compacted using a vibrator, then 16 model piles were set at their prescribed positions (see Photo 1). Dry sand was poured in 0.3 m thick layers into the container from a height of 2.4 m above the model ground surface. For each layer, water was poured into the container three or four times to strengthen the model ground. When the model ground was completed, the model concrete footing (raft) was cast in place. The relative densities of the ground in the models were set to be between 60% and 80 %.

2.2 Results of Tests

2.2.1 Raft Foundations

Figure 5 shows the relationship between the lateral load and lateral displacement of the raft foundations of Series III. The total vertical load was proportional to the maximum lateral load at about 7 mm of lateral displacement, as shown in Figure 6. The evaluated coefficient of friction was 0.63, calculated as the maximum horizontal load versus the vertical load in Figure 6.

2.2.2 Piled Raft foundations of small pile diameter (s/d=13)

Figure 7 shows the relationship between the lateral load and lateral displacement of piled rafts with s/d=13 and a vertical load of 32.2kN (Case2-1). The friction resistance at the raft-subsoil interface was much higher than the piles' shear force. The pile's shear force was calculated from dividing the difference between the two sectional bending moments by the distance of the two sections. The bending moments were calculated using the measured strains from a couple of strain gauges. The piles' shear force was proportional to the lateral displacement, whereas the total lateral load behavior was nonlinear.

The friction resistance of the raft was estimated by subtracting the shear forces of all 16 piles from the total lateral load.

Figure 8 shows the distributions of curvature and shear force along the piles at a lateral displacement of +7 mm, where pile B1 is, relative to the loading direction, at the front of the raft and pile B4 is at its rear. The time histories of the shear forces in piles B1, B2, B3 and B4 are shown in Figure 9. It is clear that the rear and intermediate piles carried much more lateral load than the front piles, particularly at large lateral displacements.

During loading, the sum of the axial forces of the piles changed considerably at large lateral displacements, as shown in Figure 10. The piles experienced pulling forces and the contact earth pressure beneath the raft became larger than its initial value of 22.0 kPa (=32.2 kPa × initial raft sharing ratio of 0.68). Consequently, it appears that the soil modulus (coefficient of subgrade reaction) in front of the rear and intermediate piles probably increased.

2.2.3 Pile Groups of small pile diameter (s/d=13)

Figure 11 shows the relationship between lateral load and lateral displacement for pile groups (Case2-3) with no vertical load. Figure 12 shows the distributions of curvature and shear force along the piles at a lateral displacement of +7 mm.

Table 2 Test cases and test conditions

Series of tests	Type of foundation	Test name	pile space／pile diameter (s/d)	Maximum lateral disp. (mm)	Total Vertical load (kN)	Vertical load sharing ratio (%)		Material of model piles
						pile	raft	
I	pile groups	Case2-4	13	7	32.2	97～100	3～0	Aluminum pipe φ19mm
		Case2-3	13	7	-0.1	100	0	
model ground set-up								
II	piled raft	Case2-1	13	7	32.2	32～42	68～58	Aluminum pipe φ19mm
		Case2-2	13	7	8.2	26～18	74～82	
			13	7	32.2	30～40	70～60	
model ground set-up								
III	raft	Case1-1	—	7	32.2	0	100	—
		Case1-2	—	7	12.6	0	100	—
		Case1-3	—	7	22.4	0	100	—
		Case1-4	—	5	61.6	0	100	—
model ground set-up								
IV	single pile	Case5	*	—	0.0	100	0	vinyl chloride pipe φ76mm
	piled raft	Case3-1	3.3	7	32.2	53～55	47～45	
	pile groups	Case3-3	3.3	7	0.0	100	0	
	piled raft	Case3-2	3.3	7	64.5	28～38	72～62	

The lateral load was shared almost equally among all piles regardless of location and no difference was observed between the forces on the front and rear piles, differing from Case2-1, which was a trivial indication of what effect grouping the piles would have. The reason for this is that the soil modulus (coefficient of subgrade reaction) was almost same everywhere below the raft.

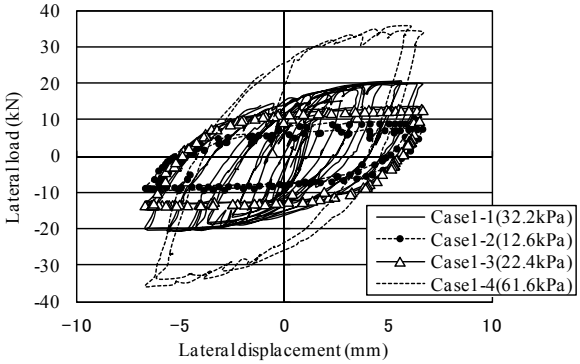

Figure 5 Lateral displacement versus lateral force of raft foundations

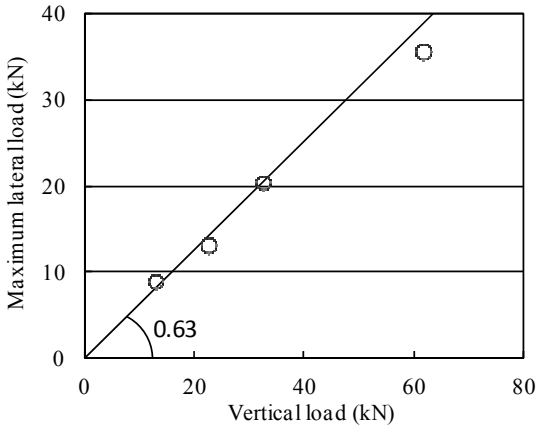

Figure 6 Vertical load versus maximum lateral load of raft foundations

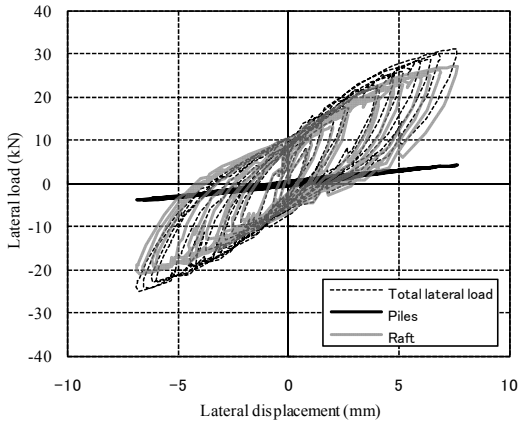

Figure 7 Lateral displacement versus lateral force of piled rafts (Case2-1)

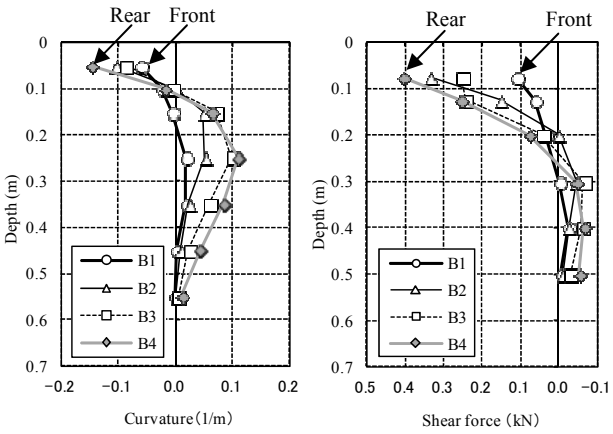

Figure 8 Distribution of curvatures and shear forces in piles of B-line (Case2-1)

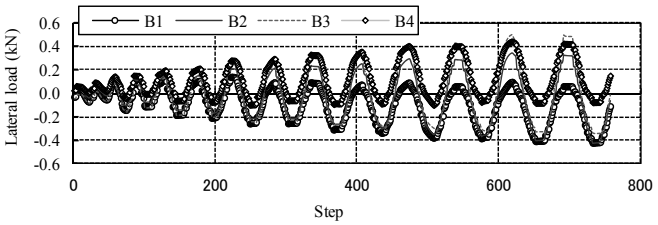

Figure 9 Time history of shear force on pile head (Case2-1)

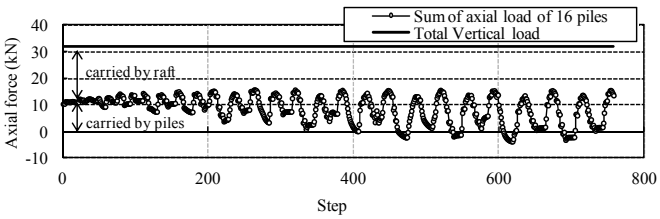

Figure 10 Time history of axial force at pile head (Case2-1)

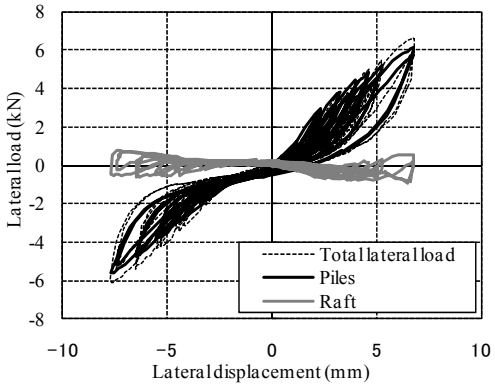

Figure 11 Lateral displacement versus lateral force of pile groups (Case2-3)

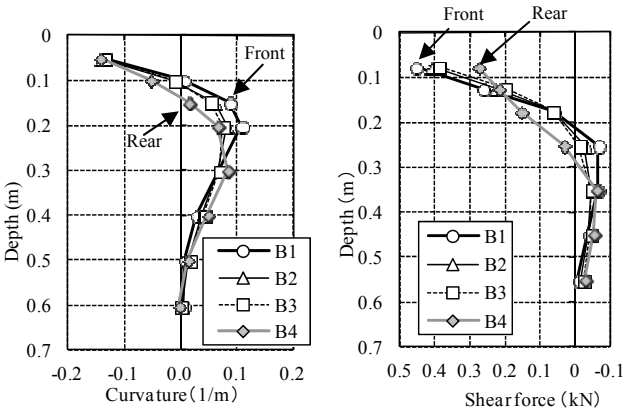

Figure 12 Distribution of curvatures and shear forces in piles of B-line (Case2-3)

2.2.4 Piled Raft foundations of large pile diameter (s/d=3.3)

Figure 13 shows the relationship between the lateral load and lateral displacement of piled rafts with s/d=3.3 and a vertical load of 32.2kN (Case3-1). The friction resistance at the raft-subsoil interface was higher than the piles' shear force, which was proportional to the lateral displacement, similar to the previously noted small diameter (s/d=13) pile case (Case2-1). Figure 14 shows the distribution of curvature and shear force along the piles at a lateral displacement of +7 mm, where pile B1 is at the front of the raft and pile B4 is at its rear. The difference between the forces carried by the rear and front piles was not significant because two opposing phenomena offset each other. The soil modulus in front of the rear piles was larger than that of the front piles, similar to piled rafts Case 2-1, whereas the front piles carry much more lateral load than the rear piles due to the effect of the tighter spacing of the piles when s/d=3.3.

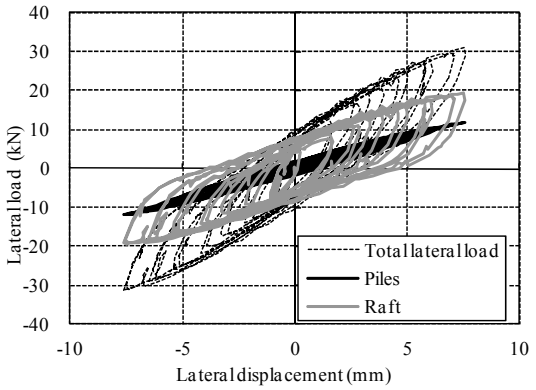

Figure 13 Lateral displacement versus lateral force of piled raft (Case3-1)

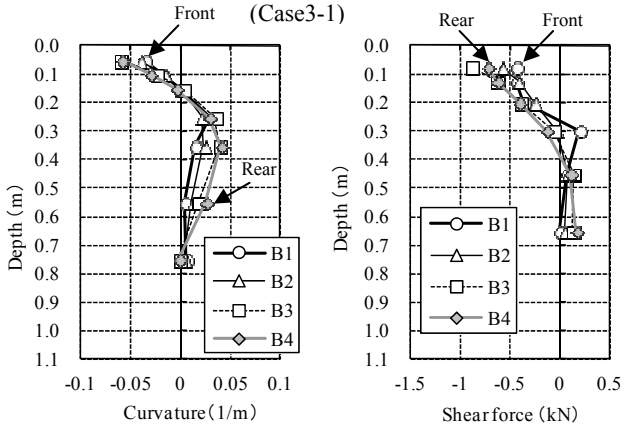

Figure 14 Distribution of curvatures and shear forces in piles of B-line (Case3-1)

2.2.5 Pile Groups of large pile diameter (s/d=3.3)

Figure 15 shows the relationship between the lateral load and lateral displacement of pile groups (Case3-3) with no vertical load. There was slight friction resistance at the raft-subsoil interface, estimated by subtracting the shear forces carried by all 16 piles from the total lateral load, which occurred because of the actual earth pressure beneath the raft.

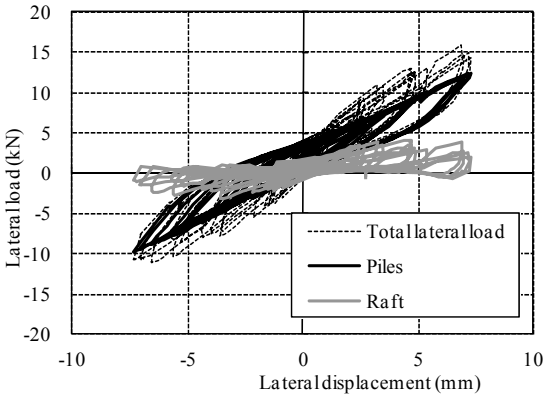

Figure 15 Lateral displacement versus lateral force of pile groups (Case3-3)

Figure 16 shows the distributions of curvatures and shear forces along the piles at a lateral displacement of +7 mm. Pile B1, at the front, carried more shear force than intermediate piles B2 and B3 or rear pile B4 because of the group effect.

There have been a lot of analytical studies and experimental studies of pile group effect on lateral resistance. Comodromos & Papadopoulou (2012) analyze the group effect of a 4x4 configuration of piles with s/d ratio of 3.0 and 9.0. Their results show tendencies similar to our results.

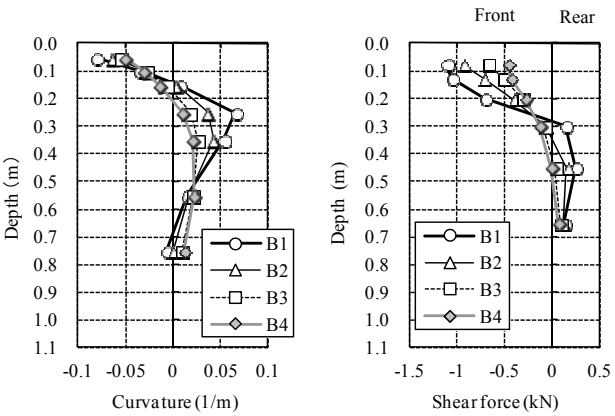

Figure 16 Distribution of curvatures and shear forces in piles of B-line (Case3-3)

2.3 Remarks

Figure 17 illustrates the lateral displacement-related distribution of lateral loads on piled rafts (Case2-1) on the pile groups and the raft in the positive loading direction. Filled circles denote the experimental results at different loading levels, solid lines show approximate curves calculated using the least squares method and the dashed line indicates the sum of the approximate resistance curves of pile groups and raft foundations. The results for the raft foundation of Case1-3, in which the contact earth pressure was 22.4 kPa, were adjusted to a contact pressure of 21 kPa because the lateral resistance of the raft foundations depended on the contact earth pressure (21 kPa = 32.2kPa×raft sharing ratio of 0.68~0.58) as in Case2-1 which modeled piled rafts.

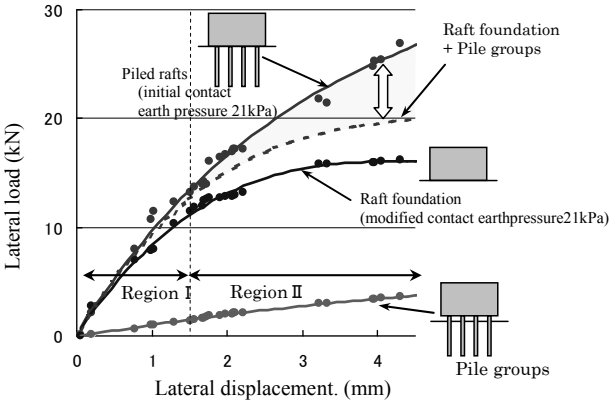

Figure 17 Comparison of lateral resistance between pile rafts, rafts, pile groups

When lateral displacement is less than about 1.5mm, the lateral resistance of the piled raft is similar to the sum of the separate lateral loads of the piles and raft. However, at higher displacements, the resistance of the piled rafts is larger than the sum of the separate lateral loads of the raft and pile groups, which means that the friction resistance increased as the contact earth pressure increased at large displacements, as shown in Figure 18. The earth pressure might have undergone an incremental change due to a possible positive dilatancy of the soil deposit and/or piles that behaved like anchors.

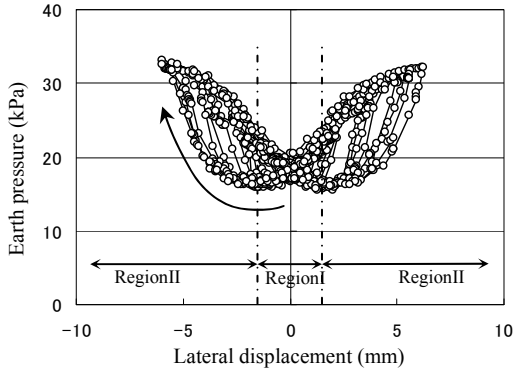

Figure 18 Lateral displacement versus contact earth pressure beneath raft

Figure 19 shows the relationship between the contact earth pressure beneath the raft and the raft's lateral resistance for the tested piled raft foundations. The friction resistance, which depended on earth pressure, did not take effect as it did for raft foundations because the contact earth pressure beneath the raft increased along the inclination line of the coefficient of friction (0.63) as shown in Figure 6.

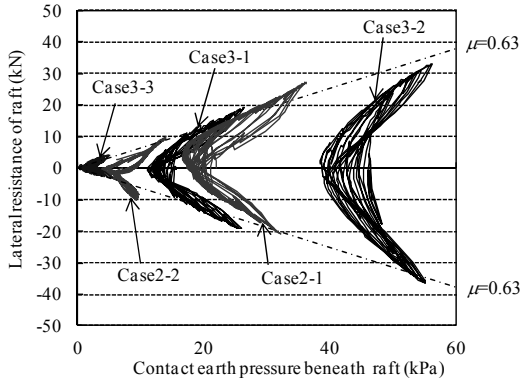

Figure 19 Contact earth pressure beneath raft versus lateral resistance of raft

3. ANALYTICAL METHOD FOR PILED RAFTS SUBJECTED TO LATERAL LOAD

3.1 Simplified Analytical Method based on Mindlin's Solution

As previously mentioned, most of the lateral load for the piled raft foundations was transferred to the soil through the raft by friction. Bending moments in the piles were caused not only by shear force at the piles' heads but also by ground displacement through raft friction. A simplified analytical method that considers these phenomena would be useful for seismic design. Analytical methods using computer programs for piled rafts based on Mindlin's solution (Mindlin, 1936) have been developed by Kitiyodom and Matsumoto (2002, 2003), Mano and Nakai (2000, 2001) and Tsuchiya et al. (2002). In their programs, a hybrid model was employed in which the flexible raft was modeled as a thin plate, the piles as elastic beams, and the soil as interactive springs.

Kitiyodom and Matsumoto (2003) used a weighted average modulus to compute the responses of piled rafts in multi-layered soils although the theory of the method assumed an elastic linear homogeneous half space based on Mindlin's solution. Mano and Nakai (2001) applied Mindlin's solution for non-linear soils by estimating each layer's shear deformation.

The model the authors have developed (Figure 20) expands on the response to nonlinear fields and adds features as indicated bellow.

1. Pile-soil-pile and pile-soil-raft interactions are incorporated into the model. Ground deformations caused by the lateral ground reaction on an arbitrarily pile and friction between the raft and subsoil are taken into account based on Mindlin's solution. The lateral resistance of piles is calculated using the elastic beam equation for ground deformations.
2. Multi-layered soil deposits are incorporated into the model. The model for the ground is divided into many layers. The shear modulus G_j is set for each layer j. The ground displacement of the bottom layer is calculated using the semi-infinite elastic theory (Mindlin's solution), and that of an arbitrarily layer is calculated starting from the bottom and moving upward, integrating the relative displacement on each divided layer.
3. The model incorporates nonlinear soil deposits. The relationship between the shear modulus and shear strain G-γ is set for each layer. The shear strain γ of an arbitrary layer is calculated by the relative displacement between the layers just above and below it divided by the thickness of the layer (Δh_j). The equivalent shear modulus of an arbitrary layer is used to estimate the effect of pile-soil-pile and pile-soil-raft interactions.
4. The model incorporates nonlinearity of the coefficient of lateral subgrade reaction of piles (k_h). The stiffness of the reaction between a pile and soil at an arbitrary depth decreases as their relative displacement. The decrease in stiffness is considered to occur only around piles.
5. Pile material nonlinearity is incorporated into the model. The relationship between bending moment and curvature (M- ϕ) is considered, depending on the axial load on the piles.

The procedure of the analysis is shown in Figure 21. i) First, the lateral temporary loads for the piles and the raft are set as F_p and F_r respectively. ii) The ground displacement δ_{rp} and the displacement of the raft (footing) δ_{rr} induced by F_r are calculated based on Mindlin's solution, taking the nonlinearity of the soil deposits into consideration. iii) Next, the lateral displacement δ_{hp} and subgrade reaction R_{hp} of each pile are estimated using the elastic beam method based on the values δ_{rp} and F_p. iv) Then, the ground displacement at other piles' positions δ_{pp} and the displacement of the raft δ_{pr} induced by R_{hp} are calculated based on Mindlin's solution. v) The total displacement of the raft δ_r ($=\delta_{gr(0)} = \delta_{rr} + \delta_{pr}$) should be the same as the displacement at the piles' heads δ_{hp} at z=0. If δ_r differs

from δ_{hp} , then the above calculations are repeated by resetting F_p and F_r.

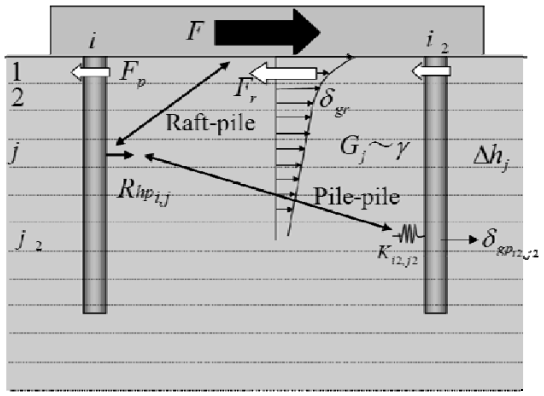

Figure 20 Developed analytical model for piled rafts subjected to lateral load

Equation (2) shows the lateral displacement of each component with a flexibility matrix where α_{pipj}, α_{ririj}, α_{pirj} and α_{ripj} are interaction factors, and K_{pi}, and K_{ri} are the stiffness of the pile and the raft. The flexibility matrix follows Randolph (1983). Each flexibility component ($1/K_p$, etc) isn't calculated in our procedure. In step iii), the displacement of the pile heads, δ_{hp} is calculated directly considering pile head shear forces, ground displacements induced by raft friction and ground displacements induced by other piles' reaction forces.

$$\begin{pmatrix} \delta_{hp1} \\ \delta_{hp2} \\ \delta_{hp3} \\ \vdots \\ \delta_{hpn} \\ \delta_{r1} \\ \delta_{r2} \\ \delta_{r3} \\ \vdots \\ \delta_{rm} \end{pmatrix} = \begin{pmatrix} 1/K_{p1} & \alpha_{p1p2}/K_{p2} & \cdots & \alpha_{p1rl}/K_{r1} & \alpha_{p1r2}/K_{r2} & \cdots & \alpha_{p1rm}/K_{rm} \\ \alpha_{p2p1}/K_{p1} & 1/K_{p2} & \cdots & \alpha_{p2rl}/K_{r1} & \alpha_{p2r2}/K_{r2} & \cdots & \alpha_{p2rm}/K_{rm} \\ \alpha_{p3p1}/K_{p1} & \alpha_{p3p2}/K_{p2} & \cdots & \alpha_{p3rl}/K_{r1} & \alpha_{p3r2}/K_{r2} & \cdots & \alpha_{p3rm}/K_{rm} \\ \vdots & \vdots & & \vdots & \vdots & & \vdots \\ \alpha_{pnp1}/K_{p1} & \alpha_{pnp2}/K_{p2} & \cdots & \alpha_{pnrl}/K_{r1} & \alpha_{pnr2}/K_{r2} & \cdots & \alpha_{pnrm}/K_{rm} \\ \alpha_{r1p1}/K_{p1} & \alpha_{r1p2}/K_{p2} & \cdots & 1/K_{r1} & \alpha_{r1r2}/K_{r2} & \cdots & \alpha_{r1rm}/K_{rm} \\ \alpha_{r2p1}/K_{p1} & \alpha_{r2p2}/K_{p2} & \cdots & \alpha_{r2rl}/K_{r1} & 1/K_{r2} & \cdots & \alpha_{r2rm}/K_{rm} \\ \alpha_{r3p1}/K_{p1} & \alpha_{r3p2}/K_{p2} & \cdots & \alpha_{r3rl}/K_{r1} & \alpha_{r3r2}/K_{r2} & \cdots & \alpha_{r3rm}/K_{rm} \\ \vdots & \vdots & & \vdots & \vdots & & \vdots \\ \alpha_{rmp1}/K_{p1} & \alpha_{rmp2}/K_{p2} & \cdots & \alpha_{rmrl}/K_{r1} & \alpha_{rmr2}/K_{r2} & \cdots & 1/K_{rm} \end{pmatrix} \begin{pmatrix} F_{p1} \\ F_{p2} \\ \vdots \\ F_{pn} \\ F_{r1} \\ F_{r2} \\ \vdots \\ F_{rm} \end{pmatrix}$$

$$= \underbrace{\begin{pmatrix} F_{p1}/K_{p1} + & F_{p2}\alpha_{p1p2}/K_{p2} + & \cdots \\ F_{p1}\alpha_{p2p1}/K_{p1} + & F_{p2}/K_{p2} + & \cdots \\ F_{p1}\alpha_{p3p1}/K_{p1} + & F_{p2}\alpha_{p3p2}/K_{p2} + & \cdots \\ \vdots & \vdots & \\ F_{p1}\alpha_{pnp1}/K_{p1} + & F_{p2}\alpha_{pnp2}/K_{p2} + & \cdots \end{pmatrix}}_{\text{iii), iv)}\delta_{pp}} + \underbrace{\begin{pmatrix} F_{r1}\alpha_{p1r1}/K_{r1} + & F_{r2}\alpha_{p1r2}/K_{r2} + & \cdots & F_{rm}\alpha_{p1rm}/K_{rm} \\ F_{r1}\alpha_{p2r1}/K_{r1} + & F_{r2}\alpha_{p2r2}/K_{r2} + & \cdots & F_{rm}\alpha_{p2rm}/K_{rm} \\ F_{r1}\alpha_{p3r1}/K_{r1} + & F_{r2}\alpha_{p3r2}/K_{r2} + & \cdots & F_{rm}\alpha_{p3rm}/K_{rm} \\ \vdots & \vdots & & \vdots \\ F_{r1}\alpha_{pnr1}/K_{r1} + & F_{r2}\alpha_{pnr2}/K_{r2} + & \cdots & F_{rm}\alpha_{pnrm}/K_{rm} \end{pmatrix}}_{\text{ii)}\delta_{rp}}$$

$$+ \underbrace{\begin{pmatrix} F_{p1}\alpha_{r1p1}/K_{p1} + & F_{p2}\alpha_{r1p2}/K_{p2} + & \cdots \\ F_{p1}\alpha_{r2p1}/K_{p1} + & F_{p2}\alpha_{r2p2}/K_{p2} + & \cdots \\ F_{p1}\alpha_{r3p1}/K_{p1} + & F_{p2}\alpha_{r3p2}/K_{p2} + & \cdots \\ \vdots & \vdots & \\ F_{p1}\alpha_{rmp1}/K_{p1} + & F_{p2}\alpha_{rmp2}/K_{p2} + & \cdots \end{pmatrix}}_{\text{iv)}\delta_{pr}} + \underbrace{\begin{pmatrix} F_{r1}/K_{r1} + & F_{r2}\alpha_{r1r2}/K_{r2} + & \cdots & F_{rm}\alpha_{r1rm}/K_{rm} \\ F_{r1}\alpha_{r2r1}/K_{r1} + & F_{r2}/K_{r2} + & \cdots & F_{rm}\alpha_{r2rm}/K_{rm} \\ F_{r1}\alpha_{r3r1}/K_{r1} + & F_{r2}\alpha_{r3r2}/K_{r2} + & \cdots & F_{rm}\alpha_{r3rm}/K_{rm} \\ \vdots & \vdots & & \vdots \\ F_{r1}\alpha_{rmr1}/K_{r1} + & F_{r2}\alpha_{rmr2}/K_{r2} + & \cdots & F_{rm}/K_{rm} \end{pmatrix}}_{\text{ii)}\delta_{rr}} \quad (2)$$

3.2 Simulation analyses of lateral loading tests using simplified analytical method

Simulation analyses of the lateral loading tests were carried out according to the procedure of developed analysis described in a previous chapter.

The calculated results for the raft foundation of Case1-1 of series III (Table 2) are shown in Figure 22. Figure 22(a) shows the relationship between lateral displacement and lateral load as well as the experimental results already presented in Figure 5. Figure 22(b) presents the calculated shear strain versus shear modulus, where the white circles indicate values related to the soil layer beneath the raft for each lateral load. Figure 22(c) shows the variations of lateral displacement and shear stiffness of soil deposits with the depth.

The relationship between G/G_0 and γ in Figure 4 (average curves with white squares and circles) was employed. To match the initial lateral stiffness of the raft foundations, the initial shear modulus, G_0 was decreased to 0.3 times the value given by Eq. (1). The confining pressure, σ_c is the product of overburden pressure multiplied by vertical load, as given in Table 2. The calculations agreed well with the test results.

Next, the simulations of the piled raft foundations for series II and IV (Table 2) are compared with the test results.

The employed coefficient of lateral subgrade reaction of piles k_h is given by Eq. (3). This equation is familiar to Japanese geotechnical designers, as it is presented in the Specifications for Highway Bridges in Japan (Japan Road association, 2002).

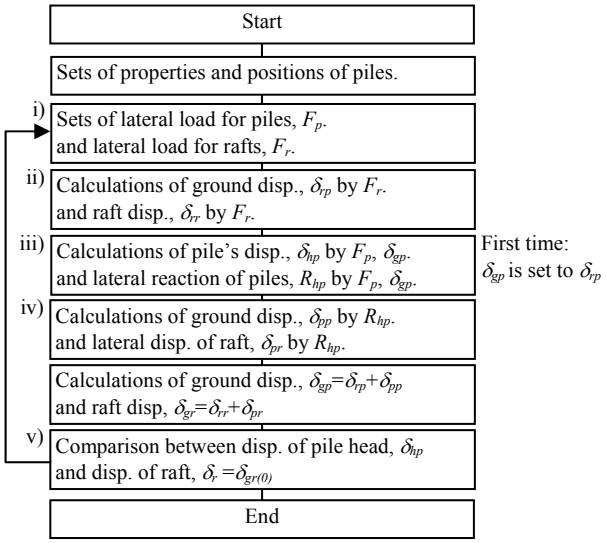

Figure 21 Procedure of developed analysis

Simulation analyses of lateral loading tests using simplified analytical method

Simulation analyses of the lateral loading tests were carried out according to the procedure of developed analysis described in a previous chapter.

The calculated results for the raft foundation of Case1-1 of series III (Table 2) are shown in Figure 22. Figure 22(a) shows the relationship between lateral displacement and lateral load as well as the experimental results already presented in Figure 5. Figure 22(b) presents the calculated shear strain versus shear modulus, where the white circles indicate values related to the soil layer beneath the raft for each lateral load. Figure 22(c) shows the variations of lateral displacement and shear stiffness of soil deposits with the depth.

The relationship between G/G_0 and γ in Figure 4 (average curves with white squares and circles) was employed. To match the initial lateral stiffness of the raft foundations, the initial shear modulus, G_0 was decreased to 0.3 times the value given by Eq. (1). The confining pressure, σ_c is the product of overburden pressure multiplied by vertical load, as given in Table 2. The calculations agreed well with the test results.

Next, the simulations of the piled raft foundations for series II and IV (Table 2) are compared with the test results.

The employed coefficient of lateral subgrade reaction of piles k_h (kN/m^3) is given by Eq. (3). This equation is familiar to Japanese geotechnical designers, as it is presented in the Specifications for Highway Bridges in Japan (Japan Road association, 1980) and Recommendations for design of building foundations (Architecture Institute of Japan, 2001).

$$k_h = 80 \times \alpha \times E_s \times d^{-3/4} \quad (3)$$

where E_s is the equivalent Young's modulus (kN/m^2), d is the pile diameter (cm), α is taken as 0.1 in consideration of the decreased

shear modulus around the piles. E_s is estimated using a modulus of $0.3G_0$ and a Poisson ratio of 0.3.

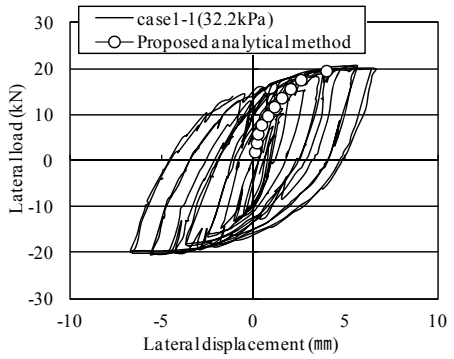

(a) Lateral displacement versus lateral force of raft foundations

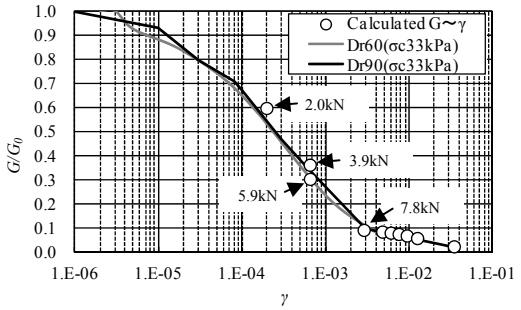

(b) Calculated shear strain versus shear modulus

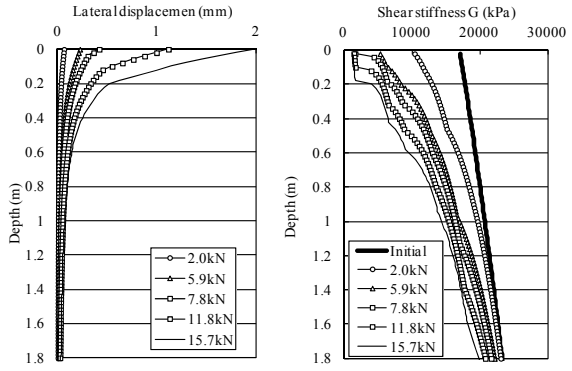

(c) Calculated distributions of lateral displacement and shear stiffness of soil deposit

Figure 22 Analytical results of raft foundation (Case1-1)

Simulated results of the lateral loading tests using developed method are shown in Figure 30 with the results of theoretical equations. The theoretical equations are presented in the next Chapter.

4. THEORETICAL EQUATIONS FOR PILED RAFTS SUBJECTED TO LATERAL LOAD

While various experiments and numerical analyses of piled raft foundations subjected to seismic loads have been conducted, simplified theoretical equations for quickly and appropriately estimating the stresses on piles and the lateral load sharing ratios between piles and rafts have not been proposed for seismic design. The first attempt should be attributed to Hamada et al. (2009, 2011). Part of these results has been presented in previous works (Hamada et al., 2012).

4.1 Approximations and assumptions for proposed theoretical equations

As illustrated in Figure 23, the lateral load F is distributed over the piles (load F_p) and the raft (load F_r) and bending moment M is caused by the shear force at piles' heads (inducing a moment M_i) and by ground displacement (inducing a moment M_g). The theoretical equations to estimate the stress of piles for seismic design of piled rafts were derived based on the model shown in Figure 24, assuming a building area basement A_r of a circular foundation with an equivalent radius $r = \sqrt{A_r / \pi}$ and making the following approximations and assumptions.

(1) The soil deposits are homogeneous. Ground displacement is derived theoretically by integration using Cerruti's solution (Eq. (5)).
(2) As to the interaction piles-soil-raft, influences related to pile-to-pile and pile-to-raft interactions are ignored. This assumption is based on the analytical results of Mano et al. (2000) and are acceptable for large pile spacing ratios.
(3) The ground displacement caused by raft friction is expressed as an exponential or polynomial function to solve the differential equation for pile deflections taking ground displacement into consideration.

Equation (4) shows the lateral displacement of each component with a flexibility matrix based on the approximations and assumptions noted above. Compare this to Eq. (2), which takes all the interactions between the piles and raft into consideration.

$$\begin{pmatrix} \delta_{hp1} \\ \delta_{hp2} \\ \delta_{hp3} \\ \vdots \\ \delta_{hpn} \\ \delta_{r1} \\ \delta_{r2} \\ \delta_{r3} \\ \vdots \\ \delta_{rm} \end{pmatrix} = \begin{pmatrix} 1/K_{p1} & 0 & \cdots & \alpha_{p1r1}/K_{r1} & \alpha_{p1r2}/K_{r2} & \cdots & \alpha_{p1rm}/K_{rm} \\ 0 & 1/K_{p2} & \cdots & \alpha_{p2r1}/K_{r1} & \alpha_{p2r2}/K_{r2} & \cdots & \alpha_{p2rm}/K_{rm} \\ 0 & 0 & \cdots & \alpha_{p3r1}/K_{r1} & \alpha_{p3r2}/K_{r2} & \cdots & \alpha_{p3rm}/K_{rm} \\ \vdots & \vdots & \cdots & \vdots & \vdots & \cdots & \vdots \\ 0 & 0 & \cdots & \alpha_{pnr1}/K_{r1} & \alpha_{pnr2}/K_{r2} & \cdots & \alpha_{pnrm}/K_{rm} \\ 0 & 0 & \cdots & 1/K_{r1} & \alpha_{r1r2}/K_{r2} & \cdots & \alpha_{r1rm}/K_{rm} \\ 0 & 0 & \cdots & \alpha_{r2r1}/K_{r1} & 1/K_{r2} & \cdots & \alpha_{r2rm}/K_{rm} \\ 0 & 0 & \cdots & \alpha_{r3r1}/K_{r1} & \alpha_{r3r2}/K_{r2} & \cdots & \alpha_{r3rm}/K_{rm} \\ \vdots & \vdots & \cdots & \vdots & \vdots & \cdots & \vdots \\ 0 & 0 & \cdots & \alpha_{rmr1}/K_{r1} & \alpha_{rmr2}/K_{r2} & \cdots & 1/K_{rm} \end{pmatrix} \begin{pmatrix} F_{p1} \\ F_{p2} \\ \vdots \\ F_{pn} \\ F_{r1} \\ F_{r2} \\ \vdots \\ F_{rm} \end{pmatrix} \quad (4)$$

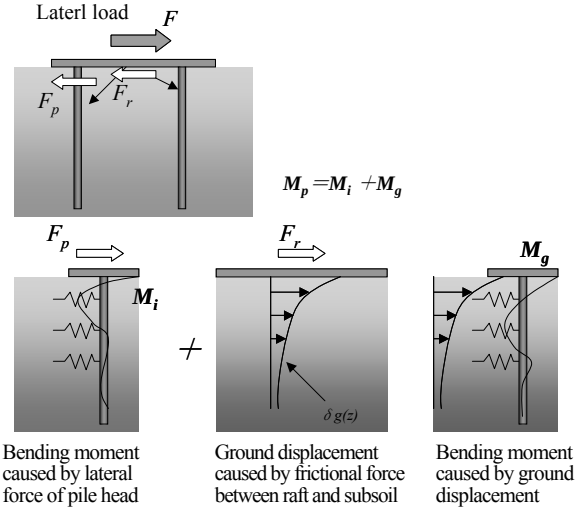

Figure 23 Mechanism of bending moments of pile in piled rafts subjected to lateral load

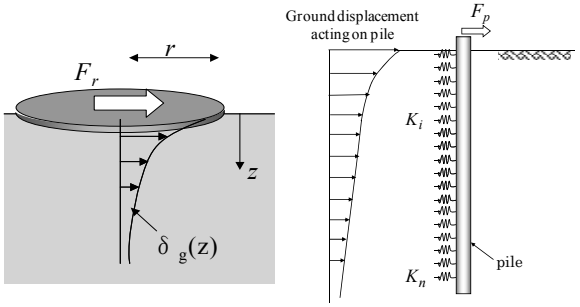

Figure 24 Simplified evaluation model for piled rafts subjected to lateral load

4.2 Ground displacement caused by frictional force between raft and subsoil

Ground displacements caused by raft friction at a given depth and at ground level are estimated by, respectively, the non-dimensional Eqs. (5) and (6) (Kanai et al. 1968). Equation (7) is an exponential function that can approximate the ground displacement. Here, δ_g is the ground displacement, $\varsigma = z/r$ is the non-dimensional depth, z is the depth, r is the equivalent radius of the building basement area, ν is Poisson's ratio, F_r is the lateral sharing load carried by the raft, G is the shear stiffness of the soil and e is the natural exponential number. Constant coefficients "a" and "b" are estimated by the least square method as 1.49 and 0.8845, respectively, having a Poisson's ratio of 0.49 and $0< \zeta <3$. Parameter "b" is expressed by $2/a(2\text{-}\nu)$ when the shear strain of the soil beneath the raft is given by τ/G. Equation (8) is another polynomial function that can also approximate the ground displacement. Coefficients "a_1", "b_1" and "c_1" are estimated by the least square method.

Figure 25 compares Eqs. (5), (7) and (8) in terms of non-dimensional depth and non-dimensional ground displacement. Equations (7) and (8) can accurately approximate Eq. (5).

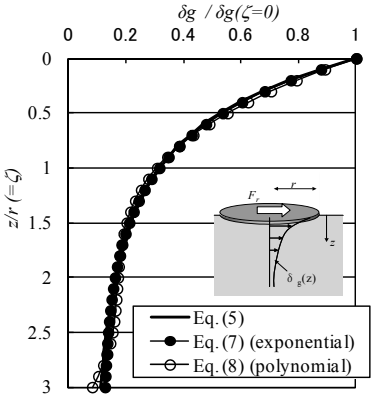

Figure 25 Relationship between non-dimensional depth and non-dimensional ground displacement

The ground displacement at the corner of building foundation can be expressed by Eqs. (7) and (8) using different coefficients (a, b or a_1, b_1, c_1).

$$\frac{\delta g(\varsigma)}{\delta g(\varsigma=0)} = \frac{1}{(2-\nu)}\left[\frac{1}{2}\ \ \frac{3+4\varsigma^2}{\sqrt{1+\varsigma^2}} - 2\varsigma + \frac{1-2\nu}{2}\left(\sqrt{1+\varsigma^2}-\varsigma\right)\right] \tag{5}$$

$$\delta g(\varsigma=0) = \frac{F_r}{2\pi G r}(2-\nu) \tag{6}$$

$$\frac{\delta g(\varsigma)}{\delta g(\varsigma=0)} = be^{-a\varsigma} + 1 - b \tag{7}$$

where $\nu = 0.49$ $\quad 0 \leqq z/r \leqq 3$

$a = 1.490$

$b = 0.8845$

$$\frac{\delta g(\varsigma)}{\delta g(\varsigma=0)} = 1 - a_1\varsigma - b_1\varsigma^2 - c_1\varsigma^3 \tag{8}$$

where $\nu = 0.49$ $\quad 0 \leqq z/r \leqq 3$

$a_1 = 1.141572$

$b_1 = -0.53329039$

$c_1 = 0.08496990$

4.3 Sectional force on piles considering ground displacement

The deflection of piles considering ground displacement is obtained by solving the differential equation expressed by Eq. (9). When ground displacement is represented by the exponential function of Eq. (7), the differential Eq. (9) is easily solved. The piles' lateral displacement is obtained mathematically from Eq. (10). The constant A_5 is obtained using Eqs. (6), (7), (9) and (10), as in Eq. (11). Constants A_1, A_2, A_3 and A_4 are determined as given in Eqs. (12), (13) and (14), respectively, based on the following assumed boundary conditions. The piles are sufficiently long, the coefficient of subgrade reaction for the piles, k_h is constant, the pile heads do not rotate, and piles and ground displacements are equal at piles' heads as well as at large depths.

$$EI\frac{d^4\delta(z)}{dz^4} = dk_h(\delta g(z) - \delta(z)) \tag{9}$$

$$\delta(z) = A_1e^{\beta(1+i)z} + A_2e^{\beta(1-i)z} + A_3e^{\beta(-1+i)z} + A_4e^{-\beta(1+i)z} + A_5e^{-\frac{a}{r}z} + \frac{F_r}{2\pi Gr}(2-\nu)(1-b) \tag{10}$$

$$A_5 = \frac{4\beta^4}{4\beta^4 + a'^4} \times b' \tag{11}$$

$$A_1 = A_2 = 0 \tag{12}$$

$$A_3 = \frac{A_5}{2}\left\{\frac{a'^4}{4\beta^4} - i\left(\frac{a'}{\beta} + \frac{a'^4}{4\beta^4}\right)\right\} \tag{13}$$

$$A_4 = \frac{A_5}{2}\left\{\frac{a'^4}{4\beta^4} + i\left(\frac{a'}{\beta} + \frac{a'^4}{4\beta^4}\right)\right\} \tag{14}$$

Here, $a' = \frac{a}{r}$, $\quad b' = \frac{F_r}{2\pi Gr}(2-\nu)b = \delta g(0) \times b$

EI : bending stiffness of pile, $\delta(z)$: horizontal displacement of pile, d : pile diametet, k_h : coefficient of subgrade reaction, $\beta = \sqrt[4]{dk_h/4EI}$, $i = \sqrt{-1}$.

$$Q(z) = a'b'\left(e^{-\beta z}\left\{\left(-\frac{a'^3}{\beta} - 2\beta^2\right)\cos\beta z - 2\beta^2\sin\beta z\right\} + a'^2e^{-a'z}\right)\left(\frac{4\beta^4}{4\beta^4 + a'^4}\right) \times EI \tag{15}$$

$$M(z) = a'b'\left(e^{-\beta z}\left\{\left(\frac{a'^3}{2\beta^2} + 2\beta\right)\cos\beta z - \frac{a'^3}{2\beta^2}\sin\beta z\right\} - a'e^{-a'z}\right)\left(\frac{4\beta^4}{4\beta^4 + a'^4}\right) \times EI \tag{16}$$

The shear force and bending moment in a pile are evaluated by Eqs. (15) and (16), respectively. These equations were derived by differentiating equation (10). The sectional shear force and bending moment in a pile head depend on the value *a'b'* which is the ground shear strain beneath the raft, as shown schematically in Figure 26, approximating ground displacement and pile displacements.

The proposed equations do not account for the vertical load. Therefore the method cannot be used in the case of second order phenomena (moment arising from the eccentricity of the vertical loading).z

4.4 Lateral load sharing ratios of piles and raft

Piles lateral resistances vary depending on the piles' positions because of the difference in earth pressure beneath the raft and/or group pile effects. However, it is assumed that the sum of the shear forces at the piles' heads is obtained by counting Eq. (15) n times for z=0, where n is the number of piles. The piles' load sharing ratio α_p, which is the ratio of the pile's sharing lateral load to the total lateral load can be expressed by Eq. (17). K_p is the lateral stiffness of the total of all the piles in a piled raft. K_r is the lateral stiffness of the raft expressed as $2\pi Gr/(2\text{-}\nu)$, derived from Eq. (6). "K_p+K_r" is used as the total lateral stiffness because "pile to raft" interactions are ignored. This equation consists of two independent parameters K_{gp}/K_r and $r\beta$. K_{gp} is n times the lateral stiffness of a single pile expressed as $4nEI\beta^3$. The parameter $r\beta$ is a non-dimensional parameter. Figure 27 shows the piles' sharing ratio α_p versus K_{gp}/K_r.

$$\alpha_p = \frac{F_p}{F} = \frac{K_p}{K_r + K_P}$$

$$= \frac{-n\frac{a}{r}b\left(-\frac{\left(a/r\right)^3}{\beta}-2\beta^2+\left(\frac{a}{r}\right)^2\right)\left(\frac{4\beta^4}{4\beta^4+\left(\frac{a}{r}\right)^4}\right)EI}{\frac{2\pi Gr}{2-\nu}-n\frac{a}{r}b\left(-\frac{\left(a/r\right)^3}{\beta}-2\beta^2+\left(\frac{a}{r}\right)^2\right)\left(\frac{4\beta^4}{4\beta^4+\left(\frac{a}{r}\right)^4}\right)EI} \quad (17)$$

$$= \frac{4nEI\beta^3 ab\left(\frac{a^3+2(r\beta)^3-a^2r\beta}{4(r\beta)^4+a^4}\right)}{\frac{2\pi Gr}{2-\nu}+4nEI\beta^3 ab\left(\frac{a^3+2(r\beta)^3-a^2r\beta}{4(r\beta)^4+a^4}\right)}$$

$$= \frac{K_{gp}/K_r\, ab\left(\frac{a^3+2(r\beta)^3-a^2r\beta}{4(r\beta)^4+a^4}\right)}{1+K_{gp}/K_r\, ab\left(\frac{a^3+2(r\beta)^3-a^2r\beta}{4(r\beta)^4+a^4}\right)}$$

4.5 Comparison of proposed equations and previous studies

Results of the simulation analyses were compared with previous studies performed using finite-element methods or elastic continuous theory based on Mindlin's solution for linear soil deposits. Table 3 shows main details of the test conditions and results of previous studies as well as calculated values based on our proposed equations (15), (16) and (17).

Figures 28 and 29 compare the lateral load sharing ratios of piles and bending moments at piles heads of the previous studies and the proposed equations.

The employed coefficient of lateral subgrade reaction of pile k_h is given by Eq. (18). In a multi-layered soil deposit, the selected value of the equivalent soil modulus, E_s is taken as the value near the pile head.

Although the proposed equations (15), (16) and (17) were derived with some assumptions and approximations, they produce results that agree well with those of previous studies.

$$k_h = \frac{1.3}{B}\frac{E_s}{1-\nu^2}\sqrt[12]{\frac{E_s d^4}{EI}} \quad (18)$$

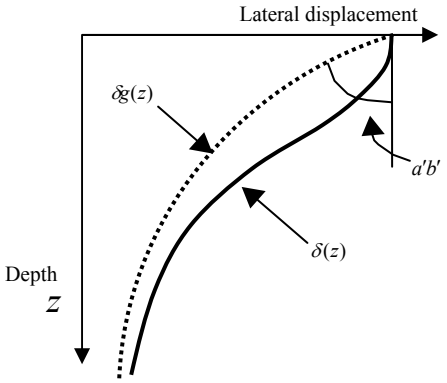

Figure 26 Schematic figure of approximate ground displacement and pile displacement

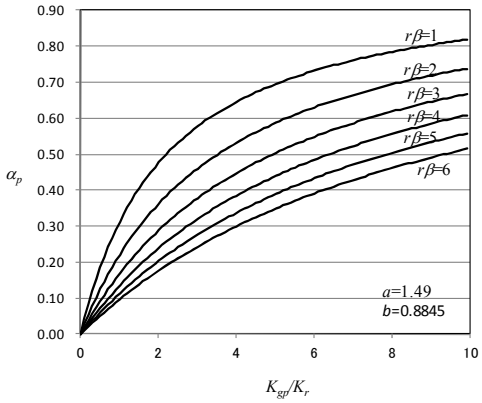

Figure 27 Piles' sharing ratio, α_p versus stiffness ratio between pile and raft, K_{gp}/K_r

4.6 Simulation analyses of lateral loading tests using theoretical equations

To confirm the validity of the derived theoretical equations, simulation analyses were performed on the lateral loading test of piled rafts described in the Chapter 2. Figure 30 shows the relationship between lateral displacement and lateral load for the theoretical equations, compared with the physical test results and the analytical results based on a multi-layered model. The initial shear modulus is taken as 0.3 times G_0 as evaluated by Eq. (1), σ_c is the product of overburden pressure multiplied by the vertical load sharing ratio of the raft (see Table 2). A coefficient of lateral subgrade reaction on pile, k_h is employed in Eq. (3) in the same way as in the simulations based on our simplified analytical method. And the shear stiffness of soil deposits are considered to decrease with the shear force just beneath the raft, $G/G_0 = 1/(1+\alpha(\tau/G_0)^\chi)$ (Ramberg-Osgood model (Jennings, 1964), Eq. (19), (20) and (21)). Here, h_{max} is a damping coefficient and $\gamma_{0.5}$ is the shear strain at G/G_0=0.5. They are set at h_{max}=0.25 and $\gamma_{0.5}$=0.00026. The relationship between shear strain, γ and normalized shear modulus, G/G_0, of the Ramberg-Osgood model, compared to the model sand, is overlaid in Figure 4.

Table 3 Conditions and results of previous analytical studies and proposed equations

Analytical Cases		Width of foundation (m)		Pile diameter d (m)	Number of piles n	Pile space/pile diameter s/d	Soil modulus Es (kN/m^2)	Poasson ratio of soil	Bending stiffness of pile EI (kNm^2)	Coefficient of subgrade reaction k_h (kN/m^3)	β (1/m)	$r\times\beta$	Analytical results		Proposed equations Eq.(15), (16)		Lateral load sharing ratio of piles αp	
		Lx	Ly										Q (kN)	M (kNm)	Q (kN)	M (kNm)	Analyses	Proposed Eq (17)
Mano and Nakai (2000)	4P-8000	12	12	0.6	4	10	257	0.33	13092	381	0.26	1.74	110	307	111	331	0.31	0.31
	4P-800	12	12	0.6	4	10	2573	0.33	13092	4617	0.48	3.25	48	76	53	94	0.14	0.15
	SP-8000	6	6	0.6	1	-	257	0.33	13092	381	0.26	0.87	91	230	92	246	0.26	0.26
	SP-800	6	6	0.6	1	-	2573	0.33	13092	4617	0.48	1.62	40	60	48	76	0.11	0.14
Tsuchiya et al. (2002)	Bacis model pile-C	20	20	0.4	25	10	4000	0.33	40212	8888	0.39	4.35	33	60	34	78	0.31	0.34
	Bacis model pile-I	20	20	0.4	25	10	4000	0.33	40212	8888	0.39	4.35	19	41	34	78		
	small s/B pile-C	10	10	0.4	25	5	4000	0.33	40212	8888	0.39	2.18	65	98	66	136	0.61	0.66
	small s/B pile-I	10	10	0.4	25	5	4000	0.33	40212	8888	0.39	2.18	33	74	66	136		
	Large Es pile-C	20	20	0.4	25	10	40000	0.33	40212	107683	0.72	8.12	15	15	16	20	0.14	0.16
	Large Es pile-I	20	20	0.4	25	10	40000	0.33	40212	107683	0.72	8.12	9	10	16	20		
Kitiyodom and Matsumoto(2003)	Case1	3	3	0.4	4	3.75	7000	0.30	8796	18073	0.67	1.14	12	10	13	14	0.49	0.52
	Case2	3	3	0.4	4	3.75	7000	0.30	8796	18073	0.67	1.14	13	11	13	14	0.50	0.52
	Case3	3	3	0.4	4	3.75	14000	0.30	8796	38295	0.81	1.37	11	8	11	10	0.45	0.46
	Case4	3	3	0.4	4	3.75	28000	0.30	8796	81144	0.98	1.66	10	6	10	8	0.39	0.39
Kitiyodom and Matsumoto(2003) FEM	Case1	3	3	0.4	4	3.75	7000	0.30	8796	18073	0.67	1.14	11	6	13	14	0.51	0.52
	Case2	3	3	0.4	4	3.75	7000	0.30	8796	18073	0.67	1.14	12	10	13	14	0.54	0.52
	Case3	3	3	0.4	4	3.75	14000	0.30	8796	38295	0.81	1.37	10	5	11	10	0.44	0.46
	Case4	3	3	0.4	4	3.75	28000	0.30	8796	81144	0.98	1.66	8	2	10	8	0.37	0.39
Hamada et al. (2005)FEM	Center pile	84	47.1	1.5	40	6.4～14.5	78843	0.49	6212622	71534	0.26	9.10	618	1737	648	2356	0.26	0.19
	Corner pile	84	47.1	1.1	40	6.4～14.5	78843	0.49	1796721	97547	0.35	12.40	813	1489	350	951		

$$\gamma = \frac{\tau}{G_0}\left(1+\alpha\left(\frac{\tau}{G_0}\right)^{\chi}\right) \tag{19}$$

$$\alpha = \left(\frac{2}{\gamma_{0.5}}\right)^{\chi} \tag{20}$$

$$\chi = \frac{2\pi h_{\max}}{2-\pi h_{\max}} \tag{21}$$

In this case, the decrease in shear stiffness was considered to be similar along the whole depth, and was based only on the values of the shear strain of the soil and the coefficient of subgrade reaction of the piles just beneath the raft. The lateral displacements were overestimated because the shear stiffness was assumed to decrease not only just under the raft but also deeper than the pile toe. Compared with the analytical results of multi-layered model, the theoretical results did not all agree well with experiments. However, overall, the results obtained are acceptable in regards to their assumptions and approximations.

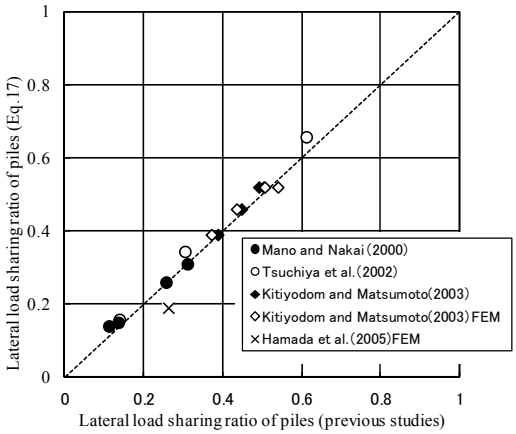

Figure 28 Comparison of calculated and measured lateral load of piles, α_p

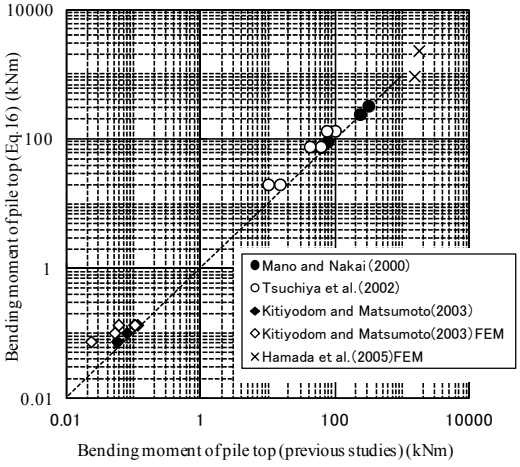

Figure 29 Comparison of calculated and measured bending moments at pile head

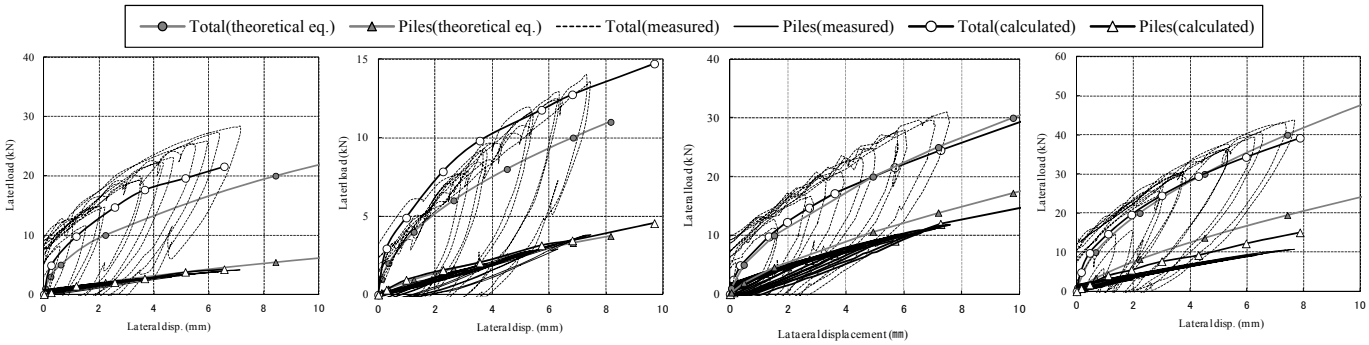

s/d=13, V=32.2kN (a) Case2-1 | s/d=13, V=8.2kN (b) Case2-2 | s/d=3.3, V=32.2kN (c) Case3-1 | s/d=3.3, V=64.5kN (d) Case3-2

Figure 30 Comparisons of calculated and measured lateral load-lateral displacement relationships

Figure 31 shows the profile of the theoretical sectional shear force and bending moment of the piles compared with test results. Piles B1, B2, B3 and B4 in the Figures correspond to the test piles shown in Figure 2, where B1 is a front pile and B4 is a rear pile. While the lateral displacements were overestimated, the sectional forces on the piles were estimated appropriately.

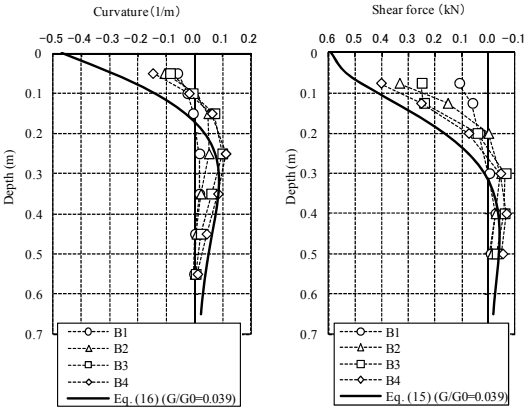

(a) s/d=13, V=32.2kN, Lateral load=30 kN（Case2-1）

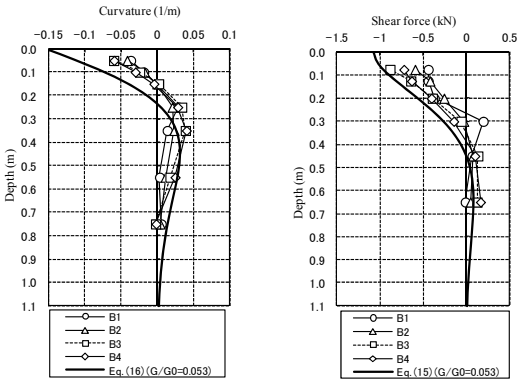

(c) s/d=3.3, V=32.2kN, Lateral load=30 kN（Case3-1）

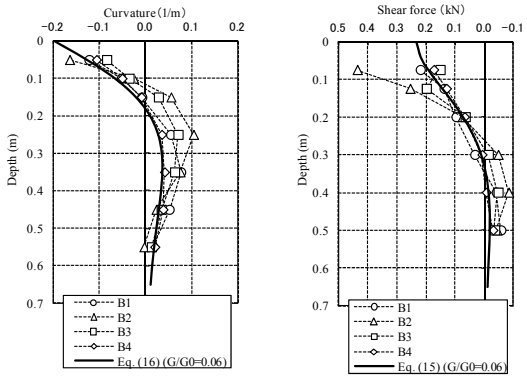

(b) s/d=13, V=8.2kN, Lateral load=11 kN（Case2-2）

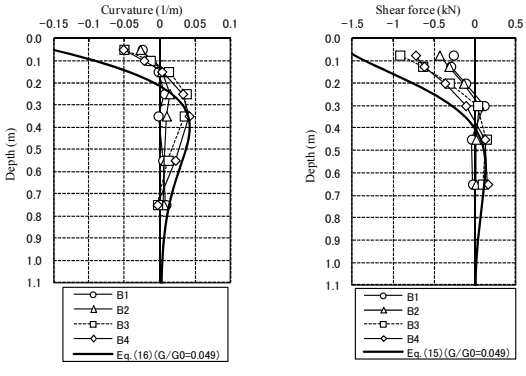

(d) s/d=3.3, V=64.5kN, Lateral load=52 kN（Case3-2）

Figure 31 Comparisons between theoretical equations and measured curvatures and shear forces

5. CONCLUSIONS

A series of experimental and analytical studies have been carried out to investigate the influence of vertical loads and pile spacing ratios on piled rafts during seismic events. Test results show that most of the lateral force is carried by raft friction when the contact pressure beneath the raft is high, and that piles experienced pulling forces on the raft, so they behave like anchors at large deformations. The sharing ratio for vertical load was one of the key factors that conditioned the lateral resistance of piled rafts.

Simulation analyses of the tested foundations were conducted using a simplified method based on Mindlin's solution, which takes pile-soil-raft interactions, multi layered soil deposits, non-linear soil deposits and non-linear pile material into consideration. The calculated results were in good agreement with the physical test results.

Based on some approximations and assumptions, simplified theoretical equations were derived to estimate the stress on piles and the lateral load sharing ratios for piles and rafts for seismic design. The sectional shear force and bending moment at the pile head depended on the ground shear strain beneath the raft. The equation for a ratio of the piles' lateral load to the total lateral load consisted of two independent parameters K_{gp}/K_r and $r\beta$.

To confirm a validity of the derived theoretical equations, simulation analyses were performed on the tested piled rafts under lateral loading. A nonlinear Ramberg-Osgood model of soil deposit was employed.

Although some assumptions and approximations were employed to derive the proposed equations, the simulated results agreed well with test results. The estimated sectional forces on the piles closely approximated the test results even when the decrease in shear stiffness was considered to be similar along the whole depth, based only on the values of the shear strain of the soil and the coefficient of subgrade reaction just beneath the raft.

6. ACKNOWLEDGMENTS

The authors are grateful to Mr. K. Nagano of Takenaka Corporation for his contribution to the experimental and analytical study.

7. REFERENCES

Architecture Institute of Japan (AIJ). 2001. Recommendations for Design of Building Foundations, 277-278 (in Japanese)

Clancy P and Randolph M.F., 1993. An approximate analysis procedure of piled raft foundations. Int J Numer Anal Methods Geomech. Vol. 17, 849-869.

Comodromos E.M. and Papadopoulou M.C., 2012. Response evaluation of horizontally loaded pile groups in clayey soils, Geotechnique, Vol. 62, No. 4, 329-39.

Hamada, J., Tsuchiya, T., Yamashita, K. and Yoshizawa M., 2005. Analytical study of stress resultant of pile on piled raft foundations during earthquake, 40th Annual Convention of Japanese Society of Soil Mechanics and Foundation Engineering, 1421-1422 (in Japanese).

Hamada, J., Tsuchiya, T. and Yamashita, K., 2009. Theoretical equations to evaluate the stress of piles on piled raft foundation during earthquake, Journal of Structural Construction Eng. (Transactions of AIJ), Vol. 74, No. 644, 1759-1767 (in Japanese).

Hamada, J., Tsuchiya, T. and Yamashita, K., 2011. Theoretical equations to evaluate the stress of piles on piled raft foundation during earthquake considering nonlinearity of soil, Journal of Structural Construction Eng. (Transactions of AIJ), Vol. 76, No. 660, 301-310 (in Japanese).

Hamada, J., Tsuchiya, T., Tanikawa, T. and Yamashita, K., 2012. Lateral loading model tests on piled rafts and their evaluation with simplified theoretical equations, IS-Kanazawa, 467-476.

Hamada, J., Shigeno, Y., Onimaru, S., Tanikawa, T., Nakamura, N. and Yamashita, K., 2014. Numerical analysis on seismic response of piled raft foundation with ground improvement based on seismic observation records, 14th International Association Computer Methods and Recent Advances in Geomechanics, 719-724.

Horikoshi, K., Matsumoto, T., Hashizume, Y., Watanabe, T. and Fukuyama, H., 2003a. Performance of piled raft foundations subjected to static horizontal loads, International Journal of Physical Modelling in Geotechnics, 3(2), 37-50.

Horikoshi, K., Matsumoto, T., Hashizume, Y. and Watanabe, T., 2003b. Performance of piled raft foundations subjected to dynamic loading, International Journal of Physical Modelling in Geotechnics, 3(2), 51-62.

Japan Road Association, 1980. Specifications for Highway Bridges - Part IV. Substructure (in Japanese).

Jennings, P.C., 1964. Periodic Response of General Yielding Structure, J.Eng. Mech. Div., ASCE, EM2, 131-163.

Kanai, K., Tajimi, H., Osawa, Y. and Kobayashi, H., 1968. Kenchiku-Kouzougaku-Taikei Jishin Kougaku, SYOUKOKUSYA, p.75 (in Japanese).

Katzenbach, R., Arslan, U. and Moormann, C., 2000. Piled raft foundation projects in Germany, Design applications of raft foundations, Hemsley J.A. Editor, Thomas Telford, 323-392.

Katzenbach, R. and Turek, J., 2005. Combined pile-raft foundation subjected to lateral loads, Proc. 16th Int. Conf. On Soil Mechanics and Geotechnical Engineering, 2001-2004.

Kitiyodom, P. and Matsumoto, T., 2002. A simplified analysis method for piled raft and pile group foundations with batter piles, International Journal for Numerical and Analytical Methods in Geomechanics, 26, 1349-1369.

Kitiyodom, P. and Matsumoto, T., 2003. A simplified analysis method for piled raft foundations in non-homogeneous soils, International Journal for Numerical and Analytical Methods in Geomechanics, 27, 85-109.

Mandolini, A., Russo, G. and Viggiani, C., 2005. Pile foundations: experimental investigations, analysis and design, Proc. 16th ICSMGE, Vol.1, 177-213.

Mano, H. and Nakai, S., 2000. An Approximate Analysis for Stress of Piles in a Laterally Loaded Piled Raft Foundation, Journal of Structural Engineering, 46B, 43-50 (in Japanese).

Mano, H. and Nakai, S., 2001. A New Simplified Nonlinear Analysis for Evaluating Stress of Piles in a Laterally Loaded Piled Raft Foundation, Journal of Structural Engineering, 47B, 427-434 (in Japanese).

Matsumoto, T., Fukumura, K., Kitiyodom,P., Horikoshi, K. and Oki, A., 2004a. Experimental and analytical study on behaviour of model piled rafts in sand subjected to horizontal and moment loading, International Journal of Physical Modeling in Geotechnics, 4(3), 1-19.

Matsumoto, T., Fukumura, K., Horikoshi, K. and Oki, A., 2004b. Shaking Table tests on model piled rafts in sand considering influence of superstructures, International Journal of Physical Modeling in Geotechnics, 4(3), 21-38.

Matsumoto, T., Nemoto, H., Mikami, H., Yaegashi, K., Arai, T. and Kitiyodom, P., 2010. Load tests of piled raft models with different pile head connection conditions and their analyses, Soils and Foundations, Vol.50, No.50, 63-81.

Mindlin, R. D., 1936. Force at a point interior of a semi-infinite solid, Physics, 7, 195-202.

Poulos, H.G., 2001. Piled raft foundations: design and applications, Geotechnique 51, No.2, 95-113.

Randlph, M.F., 1994. Design methods for pile groups and piled rafts, Proc. 13th ICSMFE, 61-82.

Tsuchiya, T., Kakurai, M., Yamashita, K. And Hamada, J., 2001. Large-scale laminar shear box for lateral pile loading tests with ground displacement, International Journal of Physical Modeling in Geotechnics 2, 43-51.

Tsuchiya, T., Nagai, H. and Ikeda, A., 2002. Analytical study on behavior of piled raft subjected to seismic load, Journal of Structural Engineering, 48B, 343-350 (in Japanese).

Watanabe,T., Fukuyama,H., Horikoshi,K. and Matsumoto,T, 2001. Centrifuge modeling of piled raft foundations subjected to horizontal loads, Proc. 5th Int. Conf. On Deep Foundation Practice incorporating Piletalk Int., 371-378.

Yamashita, K., Yamada, T. and Hamada, J., 2008. Recent case histories on monitoring settlement and load sharing of piled rafts in Japan, Proc. of the 5th International Geotechnical Seminar on Deep Foundations on Bored and Auger Piles BAP V, 181-193.

Yamashita, K., Yamada, T. and Hamada, J., 2011a. Investigation of settlement and load sharing on piled rafts by monitoring full-scale structures, Soils & Foundations, Vol.51, No.3, 513-532.

Yamashita, K., Hamada, J. and Yamada, T., 2011b. Field measurements on piled rafts with grid-form deep mixing walls on soft ground, Geotechnical Engineering Journal of the SEAGS & AGSSEA, Vol.42, No.2, 1-10.

Yamashita, K., Hamada, J., Onimaru, S. and Higashino, M., 2012. Seismic behavior of piled raft with ground improvement supporting a base-isolated building on soft ground in Tokyo, Soils & Foundations, Vol.52, No.5, Special issue on Geotechnical Aspects of the 2011 off the Pacific coast of Tohoku Earthquake, 1000-1015.